Magnetic properties of epitaxial Fe_3Si/MgO(001) thin films

Kh. Zakeri,* I. Barsukov, N. K. Utochkina, F. M. Römer, J. Lindner, R. Meckenstock, U. von Hörsten, H. Wende, W. Keune, and M. Farle
Fachbereich Physik and Center for Nanointegration (CeNIDE) Universität Duisburg-Essen, Lotharstrasse 1, 47048 Duisburg, Germany

S. S. Kalarickal† and K. Lenz
Institut für Experimentalphysik, Freie Universität Berlin, Arnimallee 14, 14195 Berlin, Germany

Z. Frait
Institute of Physics, Academy of Sciences of the Czech Republic, Na Slovance, 18221 Prague 8, Czech Republic
(Received 27 May 2007; revised manuscript received 12 October 2007; published 21 December 2007)

The composition dependence of the magnetic as well as structural properties of epitaxial 4–40 nm Fe_3Si thin films on MgO(001) have been investigated using ferromagnetic resonance, superconducting quantum interference device magnetometry, and magneto-optical Kerr effect. Magnetic anisotropy energy, g factor, and magnetization were determined for different samples with Si concentrations of 20%, 25%, or 30% at room temperature. Additionally, different annealing procedures were applied. The magnetization was determined to be on the order of $\mu_0 M \approx 1$ T. It was found that the films have a dominating cubic anisotropy $K_4 \approx 3 \times 10^3$ J/m^3 which depends on the thermal treatment of the film and is about 1 order of magnitude smaller than the one of bulk Fe. A small uniaxial in-plane anisotropy of interfacial nature was detected. The perpendicular uniaxial anisotropy term, which is dominated by an interface contribution, favors a perpendicular easy axis. From frequency-dependent ferromagnetic resonance measurements an isotropic g factor was extracted $g=2.075(5)$ for 8 and 40 nm samples and $g=2.080(5)$ for the 4 nm one. Different thermal treatments of the sample showed no influence on the g factor. The magnetic anisotropy fields and g factor decrease linearly as the Si concentration increases within the $D0_3$ regime.

DOI: 10.1103/PhysRevB.76.214421 PACS number(s): 75.30.Gw, 75.50.Bb, 75.70.Ak, 76.50.+g

I. INTRODUCTION

Fe_3Si is a ferromagnetic binary Heusler alloy[1–6] with a cubic $D0_3$ structure, a spin polarization of 43% (at $T=0$ K), and a high Curie temperature of 820 K.[7–9] These aspects make it a very promising candidate for applications in spintronics. Bulk Fe_3Si was intensively investigated theoretically[10–12] and experimentally[7–9,13] with respect to its magnetic and microstructural behaviors. In order to realize the application of Fe_3Si in future magneto-electronic and spintronic devices, the growth of well ordered ultrathin magnetic structures is required. The investigation of the epitaxial growth and magnetic properties of Fe_3Si films on semiconducting substrates has been restricted to a few groups, i.e., Fe_3Si/Si(Ge) (Refs. 14–17) and Fe_3Si/GaAs(001).[18–23] Also, the growth of Fe_3Si films on insulating substrates such as MgO(001) is of interest in connection with the tunnel magnetoresistance effect (TMR). The TMR results from the quantum mechanical tunneling with spin-split transition probabilities. The TMR can be best illustrated by the simplest system of two ferromagnetic layers separated by an insulating spacer layer. It has been predicted[24] and later demonstrated[25–27] that the TMR is enhanced just by replacing the amorphous Al_2O_3 insulating layer by a crystalline MgO barrier in ferromagnetic (FM)/MgO/FM magnetic tunneling junctions. The lattice constants of Fe_3Si and MgO are 0.567 and 0.423 nm, respectively. The lattice mismatch between MgO(001) and the Fe_3Si is 5.2% when the two lattices are rotated by 45° with respect to each other (Fe_3Si-[100]‖MgO-[110]).

In this paper, we report the structural and magnetic properties of Fe_3Si films epitaxially grown on MgO(001). After a brief overview on theoretical aspects and experimental details, the fundamental physical parameters such as magnetization, magnetic anisotropy, as well as the electronic g factor will be quantitatively determined and discussed in terms of their dependence on (i) the film thickness, (ii) different annealing procedures, and (iii) the Si concentration close to stoichiometry.

II. THEORETICAL ASPECTS

For a cubic ferromagnetic thin film, the free energy density includes the Zeeman energy, exchange energy, demagnetizing energy, the perpendicular uniaxial $K_{2\perp}$, in-plane uniaxial $K_{2\parallel}$, as well as the cubic K_4 anisotropy energy density. We assume that the sample is statically and dynamically homogeneously magnetized, i.e., we neglect the influence of exchange energy and we approximate the surface magnetic energy by an effective volume anisotropy,[28] because the values of the electrical conductivity of the material, and of the surface magnetic anisotropy for our Fe_3Si films are small (see further on).[41]

$$F = -MB[\sin\theta \sin\theta_B \cos(\phi - \phi_B) + \cos\theta \cos\theta_B] - \left(\frac{1}{2}\mu_0 M^2 - K_{2\perp}\right)\cos^2\theta + K_{2\parallel}\sin^2\theta\cos^2(\phi - \delta) + K_4 \sin^2\theta - \frac{K_4}{8}(7 + \cos 4\phi)\sin^4\theta. \quad (1)$$

Here, $\theta_B(\theta)$ and $\phi_B(\phi)$ are the polar and azimuthal angle of the external field $\vec{B}$ (magnetization $\vec{M}$) with respect to the [001] and [100] directions. δ is the angle of the in-plane uniaxial anisotropy with respect to the [100] direction (see the inset of Fig. 2).

The thickness dependence of all anisotropy terms K_i is approximated by a constant term representing a volume contribution (K_i^v) and an effective surface-interface term ($K_i^{s,\mathrm{eff}}/d$) being proportional to the reciprocal film thickness d.[42]

According to the Smit and Beljers approach,[29] the resonance condition in a ferromagnetic resonance (FMR) experiment for the out-of-plane geometry in which $\vec{B}$ is varied between the [110] and [001] directions is given by

$$\left(\frac{\omega}{\gamma}\right)^2 = \left\{B_{\mathrm{res}\perp}\cos\Delta\theta + \left[\mu_0 M_{\mathrm{eff}} + \frac{K_4}{2M} + \frac{2K_{2\parallel}}{M}\cos^2\left(\frac{\pi}{4}+\delta\right)\right]\cos 2\theta_{eq} + \frac{3K_4}{2M}\cos 4\theta_{eq}\right\}$$
$$\times\left\{B_{\mathrm{res}\perp}\cos\Delta\theta + \left[\mu_0 M_{\mathrm{eff}} + \frac{K_4}{M} + \frac{2K_{2\parallel}}{M}\cos^2\left(\frac{\pi}{4}+\delta\right)\right]\cos^2\theta_{eq} + \frac{3K_4}{M}\cos^4\theta_{eq} - \frac{2K_4}{M} + \frac{2K_{2\parallel}}{M}\sin 2\delta\right\}$$
$$-\left[\frac{K_{2\parallel}}{M}\cos\theta_{eq}\cos 2\delta\right]^2, \tag{2}$$

where $\Delta\theta=\theta_{eq}-\theta_B$, θ_{eq} is the equilibrium angle of the magnetization, and $B_{\mathrm{res}\perp}$ is the resonance field in the out-of-plane geometry. $\mu_0 M_{\mathrm{eff}}=\frac{2K_{2\perp}}{M}-\mu_0 M$ denotes the effective out-of-plane anisotropy field which includes a contribution due to the shape anisotropy and an intrinsic contribution given by $\frac{2K_{2\perp}}{M}$. Usually, the most prominent effects that contribute to $2K_{2\perp}/M$ are the breaking of the cubic crystallographic symmetry in the film (e.g., due to magneto-elastic effects) and, in general, the uniaxial surface anisotropy, both leading to an uniaxial anisotropy. While the shape anisotropy always favors an easy axis in the film plane, the intrinsic part can have positive or negative sign, i.e., lead to an easy axis in or out of the film plane.

For the in-plane configuration ($\theta_B=0$), the resonance condition becomes

$$\left(\frac{\omega}{\gamma}\right)^2 = \left(B_{\mathrm{res}\parallel}\cos\Delta\phi - \mu_0 M_{\mathrm{eff}} + \frac{K_4}{2M}[3+\cos 4\phi_{eq}] + \frac{2K_{2\parallel}}{M}\cos^2(\phi_{eq}-\delta)\right)$$
$$\times\left(B_{\mathrm{res}\parallel}\cos\Delta\phi + \frac{2K_4}{M}\cos 4\phi_{eq} + \frac{2K_{2\parallel}}{M}\cos 2(\phi_{eq}-\delta)\right), \tag{3}$$

where $\Delta\phi=\phi_{eq}-\phi_B$, ϕ_{eq} is the equilibrium angle of magnetization, and $B_{\mathrm{res}\parallel}$ is the resonance field in the in-plane geometry. In order to determine the anisotropy fields, one needs to perform a full polar and azimuthal angle dependent measurement at a fixed frequency and fit the experimental data with Eqs. (2) and (3) to obtain the magnetic anisotropy fields ($M_{\mathrm{eff}}, K_i/M,$).

For the special situation that the magnetic field is oriented in-plane along the ⟨100⟩ and ⟨110⟩ directions (easy and hard axes) and neglecting the in-plane uniaxial term, Eq. (3) simplifies to

$$\vec{B}\parallel\langle 100\rangle \Rightarrow \left(\frac{\omega}{\gamma_\parallel}\right)^2 = \left(B_{\mathrm{res}\parallel}+\frac{2K_4}{M}\right)\cdot\left(B_{\mathrm{res}\parallel}-\mu_0 M_{\mathrm{eff}}+\frac{2K_4}{M}\right), \tag{4}$$

$$\vec{B}\parallel\langle 110\rangle \Rightarrow \left(\frac{\omega}{\gamma_\parallel}\right)^2 = \left(B_{\mathrm{res}\parallel}-\frac{2K_4}{M}\right)\cdot\left(B_{\mathrm{res}\parallel}-\mu_0 M_{\mathrm{eff}}+\frac{K_4}{M}\right), \tag{5}$$

and for the [001] direction ($\vec{B}$ is applied parallel to the film normal), Eq. (2) simplifies to

$$\vec{B}\parallel[001] \Rightarrow \frac{\omega}{\gamma_\perp} = B_{\mathrm{res}\perp}+\mu_0 M_{\mathrm{eff}}+\frac{2K_4}{M}. \tag{6}$$

One should note that Eqs. (4)–(6) are only valid if $\vec{B}$ is large enough to align the magnetization parallel to its direction ($\phi_B=\phi_{eq}, \theta_B=\theta_{eq}$).

The resonance frequency squared is a parabolic function of the resonance field for the in-plane ⟨100⟩ and ⟨110⟩ directions [Eqs. (4) and (5)] and a linear function for the perpendicular configuration [$\vec{B}\parallel[001]$, see Eq. (6)]. The g factor can be precisely extracted from the quadratic term of the dependence as this term does not depend on the anisotropy fields.[30,31]

III. EXPERIMENTAL DETAILS

Epitaxial 4, 8, and 40 nm thick Fe_3Si films were grown on MgO(001) in a molecular beam epitaxy system with a base pressure of about 1×10^{-9} mbar. The MgO(001) substrate was first cleaned by isopropanol in an ultrasonic bath, afterward transferred into an ultrahigh vacuum (UHV) chamber. Inside the UHV chamber, the substrate was annealed at

1200 K for 30 min. The films were grown by coevaporation of ^{57}Fe and Si at a substrate temperature of T_s=485 K and a growth rate of about 1 nm/min, which was monitored by a calibrated quartz microbalance. In order to avoid any oxidation, the samples were capped with 5 nm of chromium. To verify that the chromium layer has no influence on the magnetic properties, also uncapped films were produced for comparison.

In addition, six different samples with the thickness of 8 nm were prepared in order to investigate the effect of annealing and Si concentration on the magnetic properties: sample A, as deposited; sample B, annealed for 1 h at T_a =900K immediately after growth at T_s=485 K in UHV; and sample C, annealed immediately after growth in UHV in steps of 100 K between T_a=550 and 900 K. At each temperature step, the sample was kept for 1 h. Sample D with a Si concentration of 20%, sample E 25%, and sample F 30% were annealed immediately after deposition in UHV at T_a =900 K for 1 h in order to obtain the $D0_3$ structure.

The structure and stoichiometry of all capped and uncapped samples were verified *ex situ* using x-ray diffraction (XRD) and energy dispersive x-ray analysis (EDX). Moreover, the actual 28% Si content of the 40 nm sample was independently confirmed by Auger electron spectroscopy sputter profiling to be 27.7% Si. Although in general the differential sputtering rarely keeps the stoichiometry, for our case, the Auger electron spectroscopy and sputter profiling investigations confirm the results of the EDX analysis. This means that for the Fe_3Si system, the sputtering rates of Si and Fe are very similar.

The FMR spectra were recorded at a microwave frequency of 9.9 GHz as a function of the polar and azimuthal angles of the external magnetic field at room temperature (RT).

The frequency dependence of the FMR spectra was investigated at RT between 1 and 70 GHz in order to precisely determine the g factor. The measurements were performed in three different geometries: $\vec{B}\|[100]$, $\vec{B}\|[110]$, and $\vec{B}\|[001]$. The measurements at 1, 4, 10, 24, and 35 GHz were performed using microwave resonators, while the additional measurements between 6 and 20 GHz and above 35 GHz were performed by placing the sample into a shorted wave guide termination.

The saturation magnetization was measured using a superconducting quantum interference device (SQUID). Magneto-optical Kerr effect (MOKE) studies were performed in longitudinal geometry to determine the coercive field as well as the magnetization reversal process. The anisotropy fields were determined by fitting the experimental FMR data of polar and azimuthal angular dependences of the resonance field by employing Eqs. (2) and (3).

IV. RESULTS AND DISCUSSION

A. Structural characterizations

We have performed x-ray diffraction measurements using Cu $K\alpha$ radiation (Fig. 1) for samples A, B, and C. The MgO(200) as well as the $Fe_3Si(200)$ and $Fe_3Si(400)$ reflexes

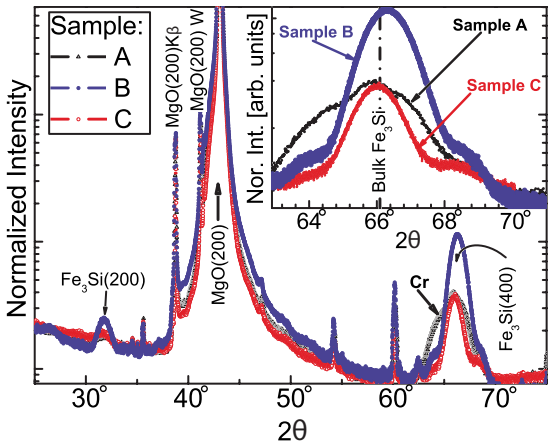

FIG. 1. (Color online) XRD spectra (logarithmic scale) of samples A, B, and C. Peaks at 60° and 54° are due to the substrate holder.

are indicated. The Cr(200) reflex of the Cr-capped sample A leads to the shoulder on the left side of the $Fe_3Si(400)$ reflex. Since no $K\beta$ filter was used, the substrate peak has a satellite due to the $K\beta$ radiation. The occurrence of a satellite due to W $L\alpha$ radiation results from a small contamination of the Cu anode. Upon comparing samples A, B, and C, one observes that samples A and C present the same diffraction angles of the Fe_3Si reflexes, while for sample B they have slightly higher values [this can be seen better in the inset, where the data of the region of the $Fe_3Si(400)$ reflex are shown]. The vertical lattice constant for sample B is $a_\perp$=0.563 nm, and 0.3% smaller than the ones of samples A and C. Samples A and C have almost bulklike lattice constants $a_\perp$=0.565 nm, whereas the lattice of sample B is slightly compressed along the film normal. This is expected in the case of epitaxial growth, since *in* the film plane, the MgO lattice constant is larger than the one of Fe_3Si, leading to a tensile strain. Sample B shows the highest intensity of the reflexes. The full widths at half maximum of all samples are, however, nearly the same, showing that the typical size of the crystallites is quite similar. The $Fe_3Si(400)$ reflex was fitted by a Lorentzian function [in the case of Cr-capped sample with two Lorentzian functions, one for Cr(200) and one for $Fe_3Si(400)$] and the average vertical size of the crystallites D=6.5±0.5 nm were calculated using the well-known Scherrer formula.[32] The crystallite sizes are the same for all samples and nearly as large as the film thickness. The higher intensity of the Bragg reflexes of sample B indicates a better (100) orientation of the crystallites and thus of the film as a whole, since only the (100) lattice planes determine the intensity in the $\theta/2\theta$ geometry. This is consistent with a larger strain within sample B due to a better orientation on the substrate. To achieve the strained state, one obviously needs a well-defined annealing procedure, since the as-prepared sample A is less strained. On the other hand, also heating too much leads to a relief of strain as observed for sample C.

In summary, the x-ray analysis yields clear evidence that sample B has the optimum epitaxial quality (see Fig. 1) with an optimum (100) orientation.

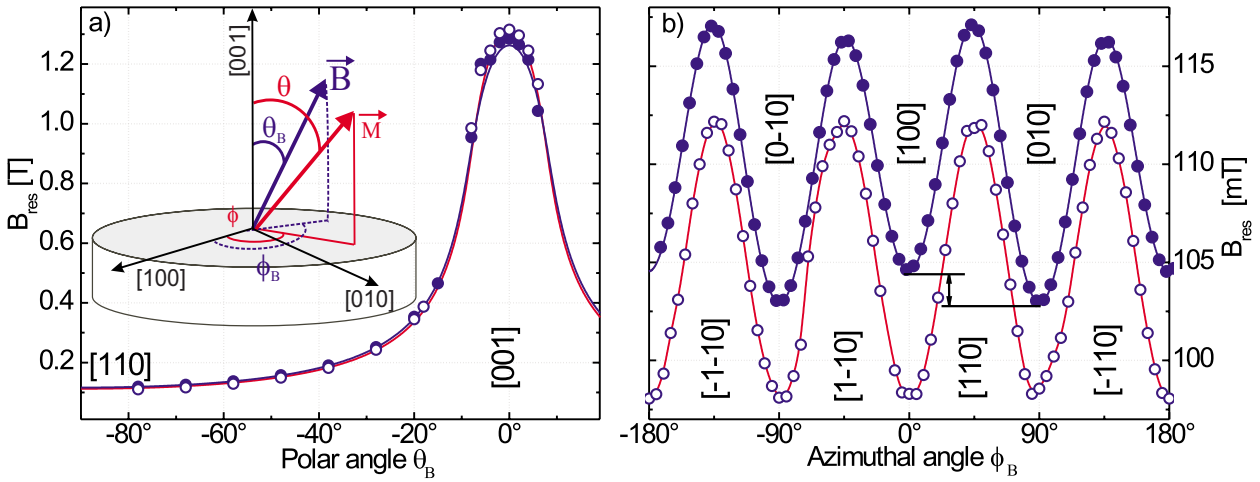

FIG. 2. (Color online) (a) Polar and (b) azimuthal angular dependences of the resonance field of a 4 nm (closed symbol) and a 40 nm (open symbol) Fe_3Si film measured at a microwave frequency of 9.9 GHz. The solid lines are fits to the experimental data. Error bars are smaller than the symbol size. The inset shows the coordinate system used for our data analysis.

B. Magnetic anisotropy

The polar and azimuthal angular dependences of the resonance field B_{res} recorded at a microwave frequency of 9.9 GHz for an as-prepared 4 and 40 nm samples are shown in Figs. 2(a) and 2(b). The 90° in-plane periodicity of the resonance field [Fig. 2(b)] confirms the expected in-plane cubic anisotropy with easy axes along the ⟨100⟩ directions of the Fe_3Si films. The cubic anisotropy field of the 4 nm sample $K_4/M=3.5$ mT is superimposed by a small uniaxial in-plane anisotropy field $K_{2\parallel}/M=0.45$ mT (see Table I) which favors an easy axis along a direction which is rotated by −13° with respect to the Fe_3Si-[100] direction. Although the origin of the uniaxial contribution could not be unambiguously extracted from the measurements, it is likely of interfacial nature, as its value decreases for thicker films. As no difference of the uniaxial in-plane anisotropy between the uncapped and Cr-capped samples was found, the cover layer as the origin can be ruled out. We therefore propose that either a small miscut of the substrate or the deposition of the Si, which is performed under an oblique angle of about 30° with respect to the film normal, are possible sources. While the former leads to a preferential step orientation on the substrate, the latter could result in a preferential alignment of the Fe atoms, or the formation of a not perfectly chemically ordered state which vanishes upon annealing.

The resulting anisotropy fields for different film thicknesses are summarized in the upper part of Table I and compared to literature data (lower part). While K_4/M was found to be almost thickness independent, the effective out-of-plane anisotropy field $\mu_0 M_{\text{eff}}$ shows a small reciprocal thickness dependence (Fig. 3). The thickness independence of K_4/M can be related to the bulklike thickness of the samples, for which the interface contributions are negligible. Our data for K_4/M are similar to the one measured by MOKE for a 21 nm Fe_3Si film on GaAs(001).[22] They are, however, smaller than the value of bulk Fe_3Si (Ref. 13) and of a 39 nm film grown on GaAs(001).[20,23]

The small thickness dependence of $\mu_0 M_{\text{eff}}=2K_{2\perp}/M-\mu_0 M$ (Fig. 3) is caused by the perpendicular uniaxial anisotropy $K_{2\perp}$ since $\mu_0 M$ is found to be thickness independent (Table I) as measured by SQUID. As the absolute value of $\mu_0 M_{\text{eff}}$ increases with increasing film thickness, $K_{2\perp}$ is positive and becomes larger for thinner films. To shed light onto the origin of $K_{2\perp}$, we distinguish surface and volume contributions according to $K_{2\perp}=K_{2\perp}^{v}+2K_{2\perp}^{s}/d$, where $K_{2\perp}^{s}$ ($K_{2\perp}^{v}$)

TABLE I. The magnetic anisotropy fields, magnetization, and the corresponding anisotropy constants of Fe_3Si films with different thickness. The error bars of the magnetization and the anisotropy terms are 10% and mainly given by the uncertainty of the sample volume.

d	Ref.	$\mu_0 M_{\text{eff}}$ (mT)	K_4/M (mT)	$K_{2\parallel}/M$ (mT)	$\mu_0 M$ (mT)	$K_{2\perp}$ (10^3 J/m^3)	K_4 (10^3 J/m^3)	$K_{2\parallel}$ (10^3 J/m^3)
4 nm	This work	−941(2)	3.5(2)	0.45(2)	1053	46.9	2.9	0.38
8 nm	This work	−958(1)	3.9(1)	0.08(1)	1052	39.4	3.3	0.07
40 nm	This work	−978(1)	3.9(1)	0.00	1059	34.1	3.3	0.00
Bulk	13 and 33	−1232	5.5		1232		5.4	
21 nm	22		4.1	0.06	931		3.1	0.046
39 nm	23	−1010	4.7	0.3	992	7	3.7	0.2

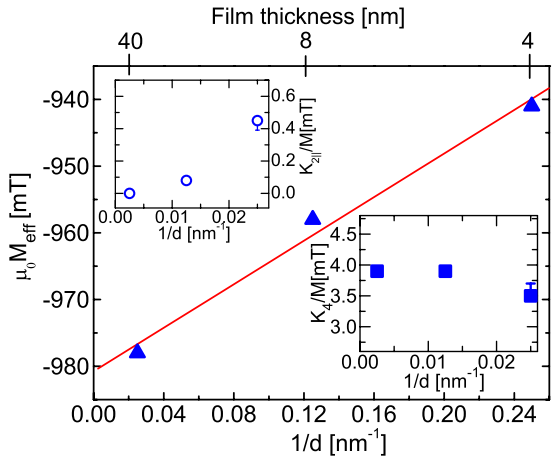

FIG. 3. (Color online) The reciprocal thickness dependence of the effective out-of-plane $\mu_0 M_{\text{eff}}$, uniaxial in-plane $K_{2\|}/M$, and cubic K_4/M anisotropy field.

is the surface (volume) contribution to $K_{2\perp}$ and d is the film thickness. Note that a simple proportionality to $1/d$ is valid only for films with thickness independent values of $K_{2\perp}^s$ ($K_{2\perp}^v$), i.e., in a coherent growth regime where no structural variations occur. According to Fig. 3 and using $\mu_0 M = 1059$ mT, the values of $K_{2\perp}^s = 3(1) \times 10^{-5}$ J/m^2 and $K_{2\perp}^v = 33(1) \times 10^3$ J/m^3 were calculated.

Both $K_{2\perp}^v$ and $K_{2\perp}^s$ are very small compared to the shape anisotropy $1/2\ \mu_0 M^2 \sim 4.4 \times 10^5$ J/m^3. The positive sign of $K_{2\perp}^v$ and $K_{2\perp}^s$ indicates that these anisotropy contributions favor an out-of-plane magnetization direction. This twofold volume anisotropy results from a tetragonal distortion of the cubic lattice[34–36] as confirmed by our x-ray analysis which shows a vertical lattice parameter for the 8 nm sample of $a_\perp = 0.563(1)$ nm, which is compressed by about 0.3% with respect to the bulk. This indicates that the lattice is still distorted even for the 8 nm sample. Due to the minimization of the elastic energy a smaller vertical value is expected due to the lattice-mismatch-induced tensile strain of Fe_3Si and MgO.

TABLE II. Magnetic anisotropy fields of $Fe_3Si/MgO(001)$ prepared by three different annealing procedures. All values are given in mT. All samples have a thickness of 8 nm. The error bar of the magnetization is 10% and mainly given by the uncertainty of the sample volume.

Sample	$\mu_0 M_{\text{eff}}$	K_4/M	$K_{2\|}/M$	$\mu_0 M$
A[a]	−958(7)	3.9(1)	0.08(1)	1052
B[b]	−1080(1)	4.5(1)	0.00	1105
C[c]	−1226(7)	8.6(1)	0.00	1252

[a]Without any annealing.
[b]Directly annealed at 900 K for 1 h.
[c]Temperature raised from 550 to 900 K in steps of 100 K (every hour).

The effect of the thermal treatment on the magnetic anisotropy was studied on samples A, B, and C (see Sec. III). In the bulk, all structural phases of Fe_3Si are stable up to a temperature of 1500 K,[9] and no temperature-induced structural transformation of our sample was observed by our x-ray diffraction study.

The polar and azimuthal angular dependencies of the resonance field for all three samples are shown in Fig. 4. The anisotropy fields resulting from fitting these dependencies are listed in Table II. $\mu_0 M_{\text{eff}}$ and K_4/M increase for the annealed samples compared to the as-prepared one (sample A). Sample C has a twice as large anisotropy K_4 as sample A. The MOKE data for samples B and C (Fig. 5) support these findings. Sample B has a smaller saturation field along [110] than sample C. Assuming a coherent rotation between the easy and hard in-plane directions, the saturation field along the [110] hard in-plane direction is given by $2K_4/M$. This

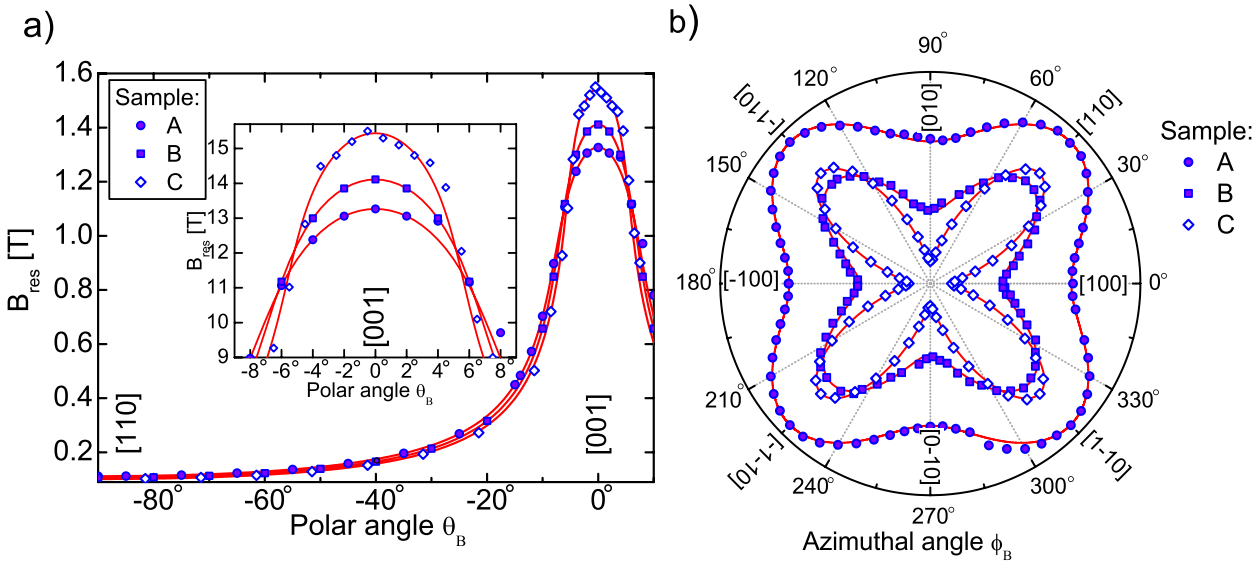

FIG. 4. (Color online) (a) Polar and (b) azimuthal angular dependences of the resonance field for samples A, B, and C. The radial scale is from 63 to 115 mT. The resulting anisotropy fields are listed in Table II.

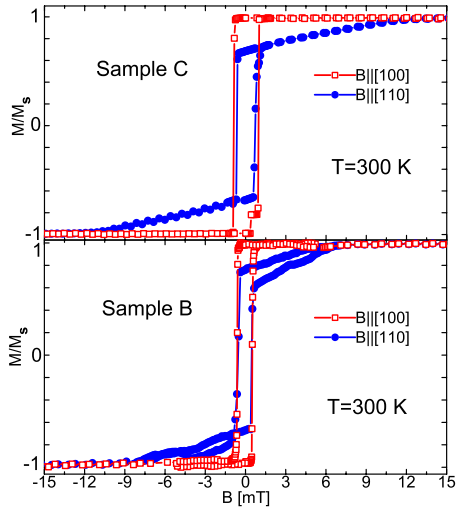

FIG. 5. (Color online) MOKE hysteresis loop of samples B and C recorded at RT with the magnetic field applied along the easy ([100]) and hard ([110]) in-plane directions.

results in anisotropy fields of $2K_4/M=9(1)$ mT for sample B, while for sample C, $2K_4/M=14(1)$ mT is obtained. Both values are consistent with the ones obtained by FMR (see Table II). In addition, sample B is magnetically softer, as can be seen from the smaller coercivity. This suggests—in combination with our x-ray analysis to be discussed below—that sample B has fewer structural defects than sample C, leading to an easier motion of the domain walls during magnetization reversal.

The influence of the Si concentration on the electronic and magnetic properties[10–12,33] is well known in the bulk. Here, we investigate the role of compositional changes in 8 nm thick $Fe_{80}Si_{20}$ (sample D), $Fe_{75}Si_{25}$ (sample E), and $Fe_{70}Si_{30}$ (sample F) films.

The magnetic anisotropy fields were determined again by performing polar and azimuthal angular dependent measurements. The results are shown in Fig. 6 for the three samples. Figure 7 shows the anisotropy fields as a function of Si concentration. The anisotropy fields of a 33 nm thick pure Fe film epitaxially grown on GaAs(001) are also shown as a reference for bulk Fe. Figure 7 shows that both $\mu_0 M_{\text{eff}}$ and K_4/M as well as the magnetization M decrease with increasing Si concentration. The magnetization of sample F is reduced by about 35% with respect to sample D and by about 15% with respect to sample E with the optimum Fe_3Si concentration (see column 6 of Table III). One should note that from the phase diagram of $Fe_{1-x}Si_x$, no crystallographic changes are expected when varying the Si concentration by 5%, as $Fe_{1-x}Si_x$ stabilizes the $D0_3$ structure at Si concentrations between 12.5% and 31%.[9] As can be seen from Fig. 7, the anisotropy fields are nearly linear with Si concentration even outside the regime of the $D0_3$ structure. By fitting the linear behavior of the anisotropy fields within the $D0_3$ regime, one obtains the concentration dependence of the anisotropy fields as K_4/M (mT)$=0.27-0.7x$ and $\mu_0 M_{\text{eff}}$ (T) $=-2.2+4x$, where x is the Si concentration in the $D0_3$ regime.

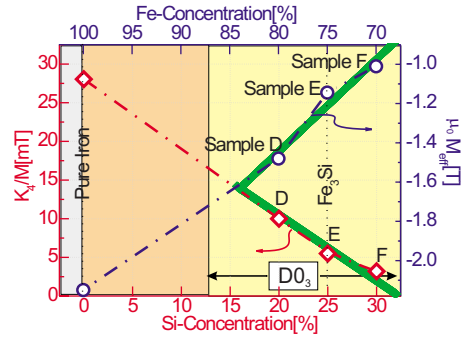

FIG. 7. (Color online) Magnetic anisotropy fields from Table III as a function of Si concentration (samples D, E, and F, respectively) measured at RT.

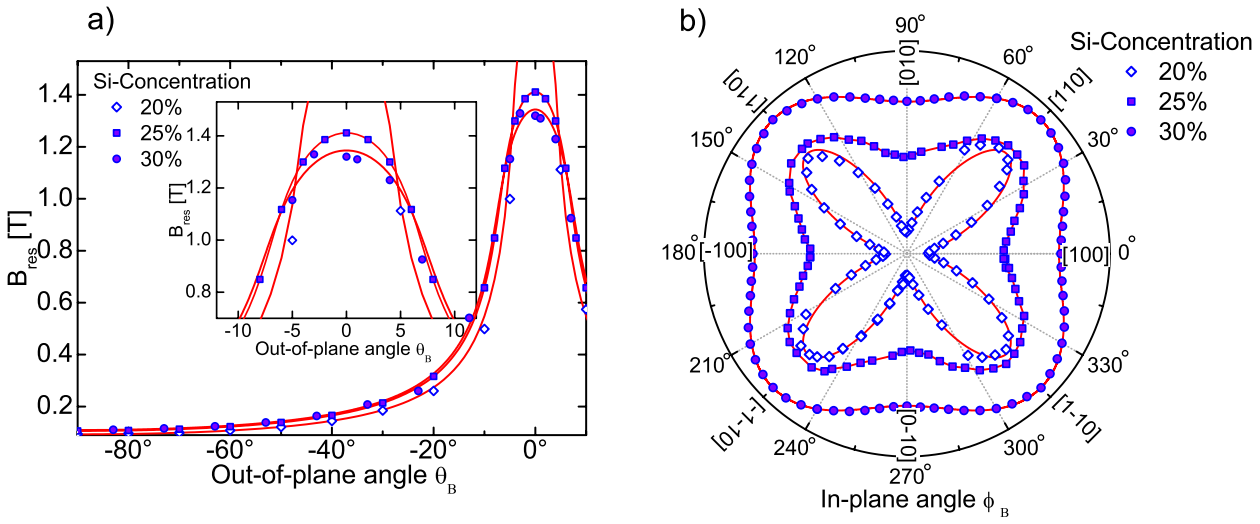

FIG. 6. (Color online) Polar (a) and azimuthal (b) angular dependence of the resonance field for different Si concentrations of 20%, 25%, and 30%. The solid lines are fits according to Eqs. (2) and (3). The radial scale is from 50 to 115 mT. The resulting anisotropy fields are listed in Table III.

TABLE III. Magnetic anisotropy fields of a 8 nm $Fe_{(1-x)}Si_x$ film with different Si concentrations x=20%, 25%, and 30% measured at RT. All values are given in mT.

Sample	Si concentration (%)	$\mu_0 M_{\text{eff}}$	K_4/M	$K_{2\parallel}/M$	$\mu_0 M$
Fe bulk	0	−2150	28.05	0.00	2150
D	20	−1460(2)	9.8	0.00	1345
E	25	−1144(3)	5.5	0.00	1105
F	30	−1006(7)	3.05	0.12	971

MOKE hysteresis loops measured along the easy axis ([100] direction) (Fig. 8) show that with increasing Si concentration, the coercivity increases from 0.3 mT for 20% Si concentration to about 1.0 mT for a Si concentration of 30%.

To explain the changes of the magnetic anisotropy as a function of Si concentration one needs to consider the following. The spin moment of the Fe and Si atoms is strongly related to their positions within the Fe_3Si lattice.[12] It is obvious that by increasing the number of Fe atoms within the cubic $D0_3$ structure of $Fe_{1-x}Si_x$, the configuration of nearest neighbors must change. The spin magnetic moment is thus expected to be influenced by the concentration. In our g-factor analysis, we will show that the orbital magnetic moment decreases with increasing Si concentration, and that this decrease is even stronger than the one of the spin magnetic moment. Taking the decrease of both spin and orbital contributions, the spin-orbit coupling itself will be smaller, which in turn explains the smaller magnetic anisotropy of the samples with higher Si content. The main origin of the change in magnetic anisotropy should thus be related to changes of the spin-orbit coupling due to a strong decrease of the spin and an even stronger decrease of the orbital magnetic moment when varying the amount of Fe and Si.

C. g factor

The g factor can be used to monitor changes in the orbital contribution to the overall magnetic moment.[30] As discussed in Sec. II, a precise determination of the g factor requires a frequency-dependent measurement. Figure 9 shows the resonance frequency squared versus the resonance field for two different crystallographic directions. The data represent the 8 nm thick Fe_3Si sample B that was annealed directly at 900 K for 1 h. The solid lines are fits according to Eqs. (4) and (5). The resonance frequency versus resonance field in perpendicular configuration $\vec{B}\|[001]$ is also shown in Fig. 9. Its linear dependence was fitted by Eq. (6). From the fits, the g factor can be extracted. The result shows that the g factor is isotropic, having a value of g=2.075(5). This is smaller than the pure bcc Fe value g_{Fe}=2.091, and also smaller than the one of other metallic ferromagnets (g_{Co}=2.187 (Ref. 37) and g_{Ni}=2.183 (Ref. 37) [or =2.25 (Ref. 38)]). The fact that the Si atoms carry a negative spin magnetic moment is well known in Fe_3Si, theoretically and experimentally (see, for example Refs. 10–12 and references therein). This, however, is not the main issue of the present paper. According to theoretical calculations,[10–12] the value of the Si spin moment is very small ($\sim -0.07\mu_B$) and therefore its contribution to the g factor is negligible. To relate the g factor to the ratio of orbital to spin magnetic moment, the well-established Kittel equation can be used. The deviation of the g factor from the free electron value for small orbital moment contributions can be written as[30,31,34]

$$g - 2 = 2\left(\frac{\mu_L}{\mu_S}\right), \tag{7}$$

where μ_S and μ_L are the spin and orbital moments, respectively. In our case, the smaller g factor is thus related to larger spin or smaller orbital contribution. As in our case the magnetization, and therefore the spin magnetic moment, is smaller than for Fe bulk, one can conclude that the smaller g factor in Fe_3Si must stem from a reduction of the orbital magnetic moment as compared to the Fe bulk case.

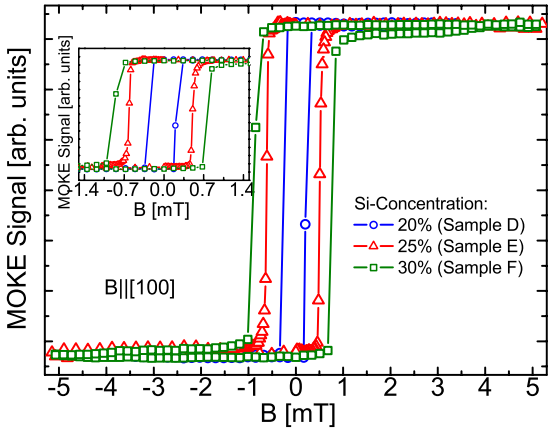

FIG. 8. (Color online) MOKE magnetization reversal loops of $Fe_{1-x}Si_x$ for different Si concentrations x=20%, 25%, and 30% measured at RT. The magnetic field was applied along the easy axis ([100] direction).

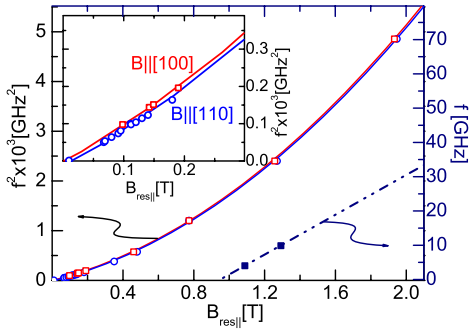

FIG. 9. (Color online) Microwave frequency squared versus the resonance field for two different in-plane configurations (left axis). The solid curves are fits according to Eqs. (4) and (5) using the anisotropy constants measured from the angular dependence of the resonance field (see Table II). The behavior of the resonance field in the perpendicular configuration, with the external magnetic field applied along the film normal, is shown by solid squares (right axis). The dash-dotted line is a fit according to Eq. (6). The inset shows the details below 0.3 T.

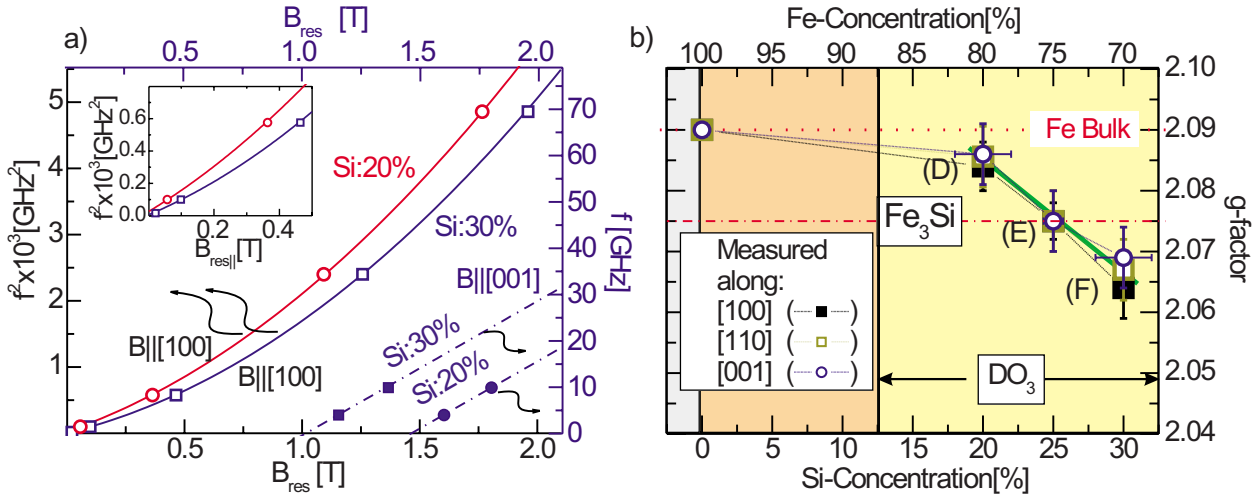

FIG. 10. (Color online) (a) The square of the microwave frequency versus the resonance field for magnetic field applied parallel to the [100] direction. The open circles and squares denote samples D and F with Si concentrations of 20% and 30%, respectively. The solid curves are fits according to Eqs. (4) and (5). The solid squares show the resonance field dependence of the resonance frequency when the external magnetic field is applied along the film normal ([001] direction). The dashed-dotted lines are the fits according to Eq. (6). The inset show the details below 0.5 T. (b) g factor for different samples with different Si concentration.

A small enhancement of the g factor was observed for the 4 nm sample $g=2.080(5)$, which can be attributed to an increase of the averaged orbital moment in the thin film regime due to the bigger contribution of larger orbital magnetic moments at the surface.

Interestingly, we found in our annealing studies on samples A, B, and C that the g factor is almost the same for all samples and very close to 2.075(5). From this, we conclude that the annealing rather reduces the number of defects than influences the local potential on an atomic level, as the latter would definitely lead to changes of the g factor. This scenario is consistent with the fact that our x-ray diffraction data do not show significant changes between the differently treated samples, neither in the half-width at half maximum of the Bragg peaks nor in their position, i.e., there are almost no changes in the lattice constant.

The results of the g factor for the off-stoichiometric samples (samples D and F) investigated at RT are shown in Fig. 10(a) together with the fitting curves according to Eqs. (4) (for the [100] direction) and (5) ([110] direction). The solid squares show the resonance field dependence of the resonance frequency when the external magnetic field is applied along the film normal ([001] direction). The dashed-dotted and dotted lines are fits according to Eq. (6). The anisotropy fields extracted from the angle-dependent measurements were used for the fitting. The g-factor as a function of the Si concentration is presented in Fig. 10(b). One observes that the g factor decreases as the Si concentration increases, indicating a reduced orbital moment. This observation can also be attributed to the change of the spin and orbital moment due to the change of the atomic configuration in the Fe-Si alloys.

V. SUMMARY

In this paper, we have investigated thin Fe_3Si films with cubic $D0_3$ structure epitaxially grown on MgO(001) substrates. The best structure was achieved at a deposition temperature of $T_s=550$ K and subsequent annealing of the film at $T=900$ K for 1 h.

The magnetic investigation by FMR, MOKE, and SQUID magnetometry on as-prepared 4–40 nm films at RT showed that the films have (a) a dominating cubic anisotropy ($K_4 \approx 3\times10^3$ J/m^3) which is about 1 order of magnitude smaller than the one of bulk Fe ($K_4=4.8\times10^4$ J/m^3), (b) a small uniaxial in-plane anisotropy,[39] and (c) a twofold out-of-plane anisotropy favoring an out-of-plane easy axis—both of interfacial nature. Extrapolating these results to thinner layers a perpendicular easy axis can be expected, if the structural homogeneity is maintained. The magnetization was found to be $\mu_0 M \approx 1$ T (bulk Fe $\mu_0 M=2.1$ T). An isotropic g factor of Fe_3Si $g=2.075(5)$ similar to the one of bulk Fe ($g=2.09$) was determined indicating the same orbital magnetism as in cubic bcc Fe.

Finally, the Si concentration dependence around the stoichiometric concentration of 25% Si:75% Fe on the magnetic properties were investigated. The g factor and magnetic anisotropy fields decrease linearly within the $D0_3$ regime.

ACKNOWLEDGMENTS

This work has been supported by the Deutsche Forschungsgemeinschaft, Sfb 491. The authors would like to thank W. Kuch for helpful discussions. One of the authors (S.S.K.) thanks K. Baberschke and the Freie Universität Berlin for their hospitality during her stay at the department. I.B. acknowledges the financial support of his stay at IP AS CR, Prague, by the EC SyntOrbMag project (MCRTN, No. MRTN-CT-2004-005567).

*zakeri@agfarle.uni-duisburg.de
†Present address: Department of Physics, Colorado State University, Fort Collins, CO 80523, USA.

[1] I. Galanakis, P. H. Dederichs, and N. Papanikolaou, Phys. Rev. B **66**, 174429 (2002); **66**, 134428 (2002).
[2] S. Fujii, S. Ishida, and S. Asano, J. Phys. Soc. Jpn. **64**, 185 (1995); S. Ishida, S. Fujii, S. Kashiwagi, and S. Asano, *ibid.* **64**, 2152 (1995).
[3] S. Picozzi, A. Continenza, and A. J. Freeman, Phys. Rev. B **66**, 094421 (2002).
[4] S. Ishida, T. Masaki, S. Fujii, and S. Asano, Physica B **245**, 1 (1998).
[5] R. A. de Groot, F. M. Mueller, P. G. van Engen, and K. H. J. Buschow, Phys. Rev. Lett. **50**, 2024 (1983).
[6] P. Webster, J. Phys. Chem. Solids **32**, 1221 (1971).
[7] V. A. Niculescu, T. J. Burch, and J. I. Budnick, J. Magn. Magn. Mater. **39**, 223 (1983).
[8] Y. Nakamura, *Alloys and Compounds of d-Elements with Main Group Elements*, Landolt-Börnstein, New Series, Group III, Vol. 19, Part C (Springer, Berlin, 1988), p. 26.
[9] T. B. Massalski, *Binary Alloy Phase Diagrams* (American Society for Metals, Ohio, 1986).
[10] E. G. Moroni, W. Wolf, J. Hafner, and R. Podloucky, Phys. Rev. B **59**, 12860 (1999).
[11] A. Bansil, S. Kaprzyk, P. E. Mijnarends, and J. Tobola, Phys. Rev. B **60**, 13396 (1999).
[12] J. Kudrnovsky, N. E. Christensen, and O. K. Andersen, Phys. Rev. B **43**, 5924 (1991).
[13] M. Goto and T. Kamimori, J. Phys. Soc. Jpn. **52**, 3710 (1983).
[14] Z. Frait (private communication).
[15] N. Onda, H. Sirringhaus, S. Goncalves-Conto, C. Schwarz, S. Zehnder, and H. von Känel, Appl. Surf. Sci. **73**, 124 (1993).
[16] M. Mendik, Z. Frait, H. von Känel, and N. Onda, J. Appl. Phys. **76**, 6897 (1994).
[17] S. Adoh, M. Kumano, R. Kizuka, K. Ueda, A. Kenjo, and M. Miyao, Appl. Phys. Lett. **89**, 182511 (2006); R. Nakane, M. Tanaka, S. Sugahara, *ibid.* **89**, 192503 (2006); T. Yoshitake, D. Nakagauchi, T. Ogawa, M. Itakura, N. Kuwano, Y. Tomokiyo, T. Kajiwara, and K. Nagayama, *ibid.* **86**, 262505 (2005).
[18] S. H. Liou, S. S. Malhotra, J. X. Shen, M. Hong, J. Kwo, H. S. Chen, and J. P. Mannaerts, J. Appl. Phys. **73**, 6766 (1993).
[19] J. Herfort, H.-P. Schönherr, and K. H. Ploog, Appl. Phys. Lett. **83**, 3912 (2003); J. Herfort, H.-P. Schönherr, K.-J. Friedland, and K. H. Ploog, J. Vac. Sci. Technol. B **22**, 2073 (2004); J. Herfort, H.-P. Schönherr, A. Kawaharazuka, M. Ramsteiner, and K. H. Ploog, J. Cryst. Growth **278**, 666 (2005).
[20] K. Lenz, E. Kosubek, K. Baberschke, J. Herfort, H.-P. Schönherr, and K. H. Ploog, Phys. Status Solidi C **3**, 122 (2006).
[21] B. Jenichen, V. M. Kaganer, J. Herfort, D. K. Satapathy, H. P. Schönherr, W. Braun, and K. H. Ploog, Phys. Rev. B **72**, 075329 (2005).
[22] A. Ionescu, C. A. F. Vaz, T. Trypiniotis, C. M. Gürtler, H. García-Miquel, J. A. C. Bland, M. E. Vickers, R. M. Dalgliesh, S. Langridge, Y. Bugoslavsky, Y. Miyoshi, L. F. Cohen, and K. R. A. Ziebeck, Phys. Rev. B **71**, 094401 (2005); A. Ionescu, C. A. F. Vaz, T. Trypiniotis, C. M. Gürtler, M. E. Vickers, H. García-Miquel, and J. A. C. Bland, J. Magn. Magn. Mater. **286**, 72 (2005).
[23] K. Lenz, E. Kosubek, K. Baberschke, H. Wende, J. Herfort, H.-P. Schönherr, and K. H. Ploog, Phys. Rev. B **72**, 144411 (2005).
[24] J. Mathon and A. Umerski, Phys. Rev. B **63**, 220403(R) (2001).
[25] D. D. Djayaprawira, K. Tsunekawa, M. Nagai, H. Maehara, S. Yamagata, N. Watanabe, S. Yuasa, Y. Suzuki, and K. Ando, Appl. Phys. Lett. **86**, 092502 (2005).
[26] S. Yuasa, T. Nagahama, A. Fukushima, Y. Suzuki, and K. Ando, Nat. Mater. **3**, 868 (2004).
[27] S. Yuasa, A. Fukushima, T. Nagahama, K. Ando, and Y. Suzuki, Jpn. J. Appl. Phys., Part 2 **43**, L588 (2004).
[28] B. Heinrich and J. F. Cochran, Adv. Phys. **42**, 523 (1993).
[29] J. Smit and H. G. Beljers, Philips Res. Rep. **10**, 133 (1955).
[30] J. Pelzl, R. Meckenstock, D. Spoddig, F. Schreiber, J. Pflaum, and Z. Frait, J. Phys.: Condens. Matter **15**, S451 (2003).
[31] A. N. Anisimov, M. Farle, P. Poulopoulos, W. Platow, K. Baberschke, P. Isberg, R. Wäppling, A. M. N. Niklasson, and O. Eriksson, Phys. Rev. Lett. **82**, 2390 (1999).
[32] B. E. Warren, in *Progress in Metal Physics*, edited by B. Chalmers and R. King (Pergamon, Oxford, 1959), pp. 147–202; *X-Ray Diffraction* (Dover, New York, 1990), Chap. 13.
[33] W. A. Hines, A. H. Menotti, J. I. Budnick, T. J. Burch, T. Litrenta, V. Niculescu, and K. Raj, Phys. Rev. B **13**, 4060 (1976).
[34] M. Farle, Rep. Prog. Phys. **61**, 755 (1998).
[35] Kh. Zakeri, Th. Kebe, J. Lindner, C. Antoniak, M. Farle, K. Lenz, T. Toliński, and K. Baberschke, Phase Transitions **79**, 793 (2006).
[36] Kh. Zakeri, Th. Kebe, J. Lindner, and M. Farle, J. Magn. Magn. Mater. **299**, L1 (2006).
[37] R. A. Reck and D. L. Fry, Phys. Rev. **184**, 492 (1969).
[38] J. R. Anderson, S. M. Bhaghat, and F. L. Cheng, Phys. Status Solidi B **45**, 357 (1971).
[39] Z. Malek and W. Schueppel, Phys. Status Solidi **2**, 136 (1962).
[40] Z. Frait and D. Fraitova, in *Frontiers in Magnetism of Reduced Dimension Systems*, NATO ASI, Series C: Mathematics and Physical Sciences edited by P. Wigen, V. Baryachtar, and N. Lesnik (Kluwer, Dordrecht, 1998), Vol. 49, pp. 121–152.
[41] In order to support this assumption, we have calculated the dynamical effects of exchange and/or conductivity and of surface anisotropy (assumed as uniaxial with symmetry axis along the sample normal) on the resonance field intensities using the "complete" FMR theory (for more details see Ref. 40). The field differences between the results of the complete theory and the above mentioned approximate one were found less than the accuracy of resonance field measurement (less than 0.1 mT) for the applied magnetic field along the film normal and parallel to the film plane for the used ranges of film thicknesses and of microwave frequencies.
[42] In publications $K_i^{s,\mathrm{eff}}$ is written as $2K_i^s$, where K_i^s is the surface anisotropy. We will also use this notation in this paper.